CHEMISTRY
A EUROPEAN JOURNAL

ChemPubSoc
Europe

DOI: 10.1002/chem.201302463

Distinct Stepwise Reduction of a Nickel–Nickel-Bonded Compound Containing an α-Diimine Ligand: From Perpendicular to Coaxial Structures

Qingsong Dong,[a] Xiao-Juan Yang,*[a, b] Shida Gong,[c] Qiong Luo,[c] Qian-Shu Li,[c] Ji-Hu Su,[d] Yanxia Zhao,[a] and Biao Wu[b]

Abstract: A nickel–nickel-bonded complex, $[\{Ni(\mu\text{-}L^{\bullet-})\}_2]$ (**1**; L = [(2,6-iPr$_2$C$_6$H$_3$)NC(Me)]$_2$), was synthesized from reduction of the $LNiBr_2$ precursor by sodium metal. Further controllable reduction of **1** with 1.0, 2.0 and 3.0 equiv of Na, respectively, afforded the singly, doubly, and triply reduced compounds $[Na(DME)_3]\cdot[\{Ni(\mu\text{-}L^{\bullet-})\}_2]$ (**2**; DME = 1,2-dimethoxyethane), $[Na(Et_2O)]Na[(L^{\bullet-})Ni{-}NiL^{2-}]$ (**3**), and $[Na(Et_2O)]_2Na[L^{2-}Ni{-}NiL^{2-}]$ (**4**). Here L represents the neutral ligand, $L^{\bullet-}$ denotes its radical monoanion, and L^{2-} is the dianion. All of the four compounds feature a short Ni–Ni bond from 2.2957(6) to 2.4649(8) Å. Interestingly, they display two different structures: the perpendicular (**1** and **2**) and the coaxial (**3** and **4**) structure, in which the metal–metal bond axis is perpendicular to or collinear with the axes of the α-diimine ligands, respectively. The electronic structures, Ni–Ni bonding nature, and energetic comparisons of the two structure types were investigated by DFT computations.

Keywords: low oxidation state · metal–metal bonding · nickel · reduction

Introduction

Bimetallic species containing a metal–metal bond have been of continuing interest since the $[Re_2Cl_8]^{2-}$ compound was reported in 1964.[1] In recent years, a number of new metal–metal bonds of s-, p- and d-block metals have been successfully synthesized with different supporting ligands.[2] When a potentially chelating ligand is used, two possible structures for the [L′MML′]-type compound may form: the coaxial and perpendicular isomers (Scheme 1). In the former structure, each ligand chelates a metal center and the metal–metal bond is (nearly) collinear with the main axes of the ligands, whereas in the latter case the ligands bridge the two metals and the M–M bond is perpendicular to the ligand axes. Although the coaxial (chelating) structure is a common motif in metal–metal-bonded complexes,[3] the perpendicular (bridging) geometry occurs mainly in some high-order (quadruple and quintuple) bonds,[4] in which the metal–metal bonding is facilitated by the bridging ligands reducing the interatomic distance. For example, the first quintuple bond complex, Ar′CrCrAr′ (Ar′ = C$_6$H$_3$-2,6-(C$_6$H$_3$-2,6-iPr$_2$)$_2$), displays a *trans*-bent geometry with weak interactions of Cr to the flanking aryl ring,[5] whereas in the subsequent dichromium analogues with *N*,*N*′-chelating ligands, the perpendicular structure is predominant with very short metal–metal distances.[4a–d] Very recently, some perpendicular Mn–Mn,[6] Fe–Fe,[4f] and Ni–Ni-bonded[7] complexes have also been reported. Moreover, theoretical studies have been carried out to compare the energies of the coaxial and perpendicular isomers.[8]

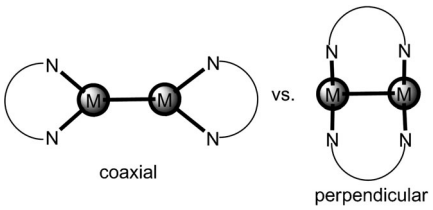

Scheme 1. The coaxial and perpendicular isomers of metal–metal-bonded compounds.

Nickel is recognized as an important element because it not only plays essential roles in many catalytic reactions[9] but also is involved in biological redox reactions performed by nickel enzymes.[10] A great number of dinickel complexes have been known, but they usually contain bridging ligands, such as in the $\{Ni_2(\mu\text{-}H)_n\}$,[11] $\{Ni_2(\mu\text{-}C)_n\}$,[12] $\{Ni_2(\mu\text{-}S)_n\}$,[13] $\{Ni_2(\mu\text{-}P)_n\}$ (n = 1, 2)[14] and $\{Ni_2(\mu\text{-arene})\}$[15] fragments. On

[a] Dr. Q. Dong, Prof. X.-J. Yang, Dr. Y. Zhao
State Key Laboratory for Oxo Synthesis and Selective Oxidation
Lanzhou Institute of Chemical Physics, CAS
Lanzhou 730000 (P.R. China)
E-mail: yangxj@lzb.ac.cn

[b] Prof. X.-J. Yang, Prof. B. Wu
College of Chemistry and Materials Science
Northwest University, Xi′an 710069 (P.R. China)

[c] S. Gong, Dr. Q. Luo, Prof. Q.-S. Li
Center for Computational Quantum Chemistry
South China Normal University, Guangzhou 510631 (P.R. China)

[d] Prof. J.-H. Su
Hefei National Laboratory for Physical Sciences at Microscale and Department of, Modern Physics, University of Science and Technology of China, Hefei 230026 (P.R. China)

Supporting information for this article is available on the WWW under http://dx.doi.org/10.1002/chem.201302463.

the other hand, unsupported Ni–Ni-bonded compounds containing low-valent, low-coordinate Ni centers may be of much interest because they can potentially display novel electronic structures and reactivity. For such species, however, only few examples with the perpendicular structure have been reported,[7] whereas the unsupported coaxial structure is unknown.[16]

In the past several years, our team has reported a series of metal–metal-bonded compounds with bulky α-diimine ligands.[17] These redox noninnocent ligands can be readily reduced to the monoanionic radical or dianion, which have proven to be able to stabilize complexes with low-valent, low-coordinate metal centers. In this current work, we employed the α-diimine ligand L (L = [(2,6-*i*Pr$_2$C$_6$H$_3$)NC(Me)]$_2$) to synthesize the dinickel analogues, and four Ni–Ni-bonded compounds (**1**–**4**) were obtained. Very interestingly, complexes **1** and **2** show the "perpendicular" structure with the α-diimine ligands spanning the Ni–Ni bond, whereas the further reduced products **3** and **4** feature the "coaxial" geometry, in which the ligands are in a chelating fashion. Herein we report the crystal structures of these compounds and their electronic structures studied by EPR and DFT calculations, as well as a comparison of the bonding nature and energy difference of the two structure types.

Results and Discussion

The nickel–nickel-bonded complexes **1**–**4** were obtained from stepwise reduction of the dibromo precursor LNiBr$_2$[18] with sodium metal (Scheme 2). Treatment of LNiBr$_2$ with

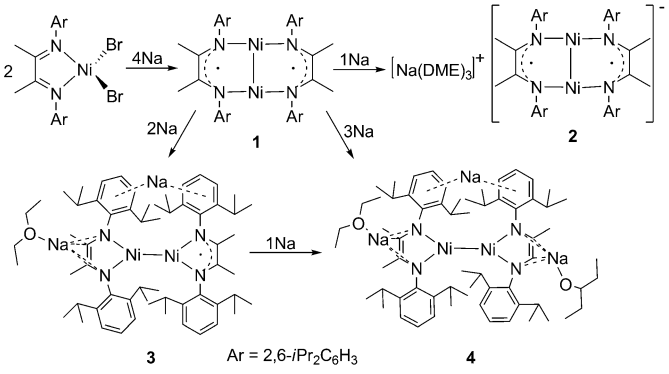

Scheme 2. Synthesis of the Ni–Ni-bonded complexes **1**–**4**.

2.0 equiv of Na in Et$_2$O afforded green crystals of the complex [{Ni(μ-L$^{\bullet-}$)}$_2$] (**1**). Subsequent reduction of **1** by 1.0 equiv of Na gave a dark-green species, [Na(DME)$_3$][{Ni(μ-L$^{\bullet-}$)}$_2$] (**2**), in which the original dinuclear {Ni$_2$}$^{2+}$ core has been reduced to the mixed-valent {Ni$_2$}$^+$, but the monoanionic ligands remain unchanged. When **1** was treated with 2.0 equiv of Na, a doubly reduced species [Na(Et$_2$O)]Na[(L$^{\bullet-}$)Ni–NiL^{2-}] (**3**) was obtained as purple crystals, wherein one of the ligands remains L$^{\bullet-}$ but the other is reduced to dianion (L^{2-}). Further reduction of the dinickel complex **3** with 1.0 equiv of Na led to a dark-brown species, [Na(Et$_2$O)]$_2$Na[L^{2-}Ni–NiL^{2-}] (**4**), in which both ligands are dianionic and one Na$^+$ ion is sandwiched between two aryl rings (note that this Na atom is disordered over two positions with 50% occupancy each). Upon removal from the mother liquor, these complexes are air- and moisture-sensitive, but are thermally stable under argon at room temperature.

[{Ni(μ-L$^{\bullet-}$)}$_2$] (1): Complex **1** shows the "perpendicular" structure with two slightly tilted six-membered heterocycles fused by the Ni–Ni bond (Figure 1). The ligands act as bridges between the two Ni atoms, and the coordination ge-

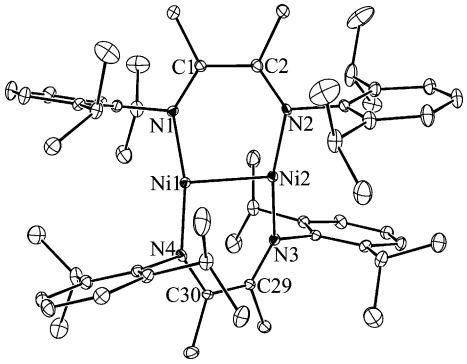

Figure 1. Molecular structure of **1** (thermal ellipsoids are set at the 20% probability level; hydrogen atoms have been omitted for clarity). Selected bond lengths [Å] and angles [°]: Ni1–Ni2 2.2957(6), Ni1–N1 1.828(3), Ni1–N4 1.836(3), Ni2–N2 1.832(3), Ni2–N3 1.832(3), N1–C1 1.340(4), C1–C2 1.416(4), N2–C2 1.346(4), N3–C29 1.337(4), C29–C30 1.434(4), N4–C30 1.329(4), N1-Ni1-N4 166.34(11), N1-Ni1-Ni2 95.04(8), N3-Ni2-Ni1 95.17(8), N2-Ni2-N3 166.82(11).

ometry around nickel can be best described as slightly distorted T-shape with each metal atom being three-coordinated by two N atoms from two different ligands as well as by the other Ni atom. This structure is similar to the perpendicular Ni–Ni,[7] Fe–Fe,[4f] Cr–Cr,[4a–d] and Mo–Mo-bonded[4e] complexes with *N*,*N*′-chelating ligands. In complex **1**, the C–N (1.346(4)–1.329(4) Å) and C–C (1.434(4) and 1.416(4) Å) bond lengths of the central C$_2$N$_2$ moiety indicate that the neutral ligand in LNiBr$_2$ has accepted one electron to form the monoanionic π radical (L$^{\bullet-}$).[19] Thus, the nickel centers should have the formal oxidation state of +1 resulting from reduction of the initial Ni^{2+} ions in LNiBr$_2$. The Ni^{I}–Ni^{I} distance of 2.2957(6) Å in **1** is almost identical to those in [{Ni(μ-κ^2-*N*,*N*′-Priso)}$_2$] (2.2908(11) Å; Priso = [{(C$_6$H$_3$*i*Pr$_2$-2,6)N}$_2$CN(*i*Pr)$_2$}])[7a] and [{Ni(μ-*N*,*N*′-Pham)}$_2$] (2.2938(12) Å; Pham = [{(SiMe$_3$)N}$_2$CPh]$^-$),[7b] which are the shortest known examples of Ni–Ni interaction.

The room-temperature EPR spectrum of complex **1** in Et$_2$O solution shows a multiline pattern (g = 2.014) corresponding to ligand-centered radicals delocalized on the NCCN atoms of the α-diimine. The experimental signal is in agreement with the simulated one (Figure S1a in the Sup-

porting Information) and is also similar to literature reports on related systems.[17c,20] In addition, the low-temperature solid-state EPR spectrum (77 K) is also in good agreement with the simulated one (Figure S1b in the Supporting Information), displaying two components at $g_{\parallel}=2.044$ and $g_{\perp}=2.012$ of the ligand radical.[21] Meanwhile, the low-temperature spectrum demonstrates that complex **1** contains a diamagnetic [$Ni^{I}Ni^{I}$] core, and thus the two nickel(I) centers are magnetically coupled through the Ni–Ni bonding.

[Na(DME)$_3$][{Ni(μ-L$^{\bullet-}$)}$_2$] (2): Further reduction of complex **1** with 1.0 equiv of Na in mixed solvents (Et_2O/DME) afforded the product **2**. The molecular structure of **2** shows the presence of an anionic [{Ni(μ-L$^{\bullet-}$)}$_2$]$^-$ unit and a solvated [Na(DME)$_3$]$^+$ countercation (Figure 2). The anionic [{Ni(μ-L$^{\bullet-}$)}$_2$]$^-$ unit is similar to that of **1**, in which the ligands act as bridges between the two Ni centers and the Ni–Ni bond is perpendicular to the main axis of the ligands. Compared with **1**, complex **2** has accepted one more electron (indicated by the incorporation of a sodium cation), implying that either a nickel center or a ligand has been reduced. An examination of the C–N (1.376(4)–1.363(4) Å) and C–C (1.384(5) and 1.370(5) Å) bond lengths revealed that both of the α-diimine ligands maintain the monoanionic π radical (L$^{\bullet-}$) form. Therefore, the single-electron reduction should have occurred to the [$Ni^{I}Ni^{I}$] core (in **1**) to form a mixed-valent [$Ni^{I}Ni^{0}$] species in **2**, although the two Ni atoms are essentially indistinguishable with very similar bond parameters around them. Moreover, this single-electron reduction of the [Ni^{I}–Ni^{I}] core caused a slight lengthening of the Ni–Ni bond from **1** (2.2957(6) Å) to **2** (2.3383(14) Å). The arrangement of the two C_2N_2 planes (dihedral angle 21.5°) is flattened in comparison to the tilted conformation in **1** (dihedral angle 39.7°).

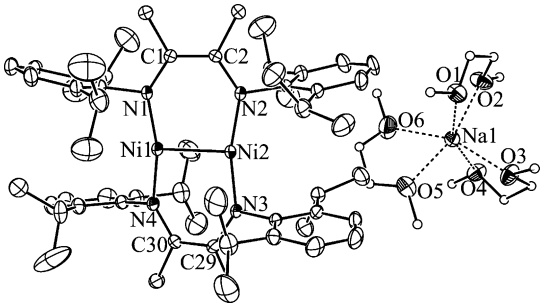

Figure 2. Molecular structure of **2** (thermal ellipsoids are set at the 20% probability level; solvent molecules and hydrogen atoms have been omitted and C atoms on DME drawn as smaller spheres for clarity). Selected bond lengths [Å] and angles [°]: Ni1–Ni2 2.3383(14), Ni1–N1 1.819(3), Ni1–N4 1.812(3), Ni2–N2 1.810(3), Ni2–N3 1.807(3), N1–C1 1.363(4), C1–C2 1.384(5), N2–C2 1.367(4), N3–C29 1.365(4), C29–C30 1.370(5), N4–C30 1.376(4), N1-Ni1-N4 164.99(12), N1-Ni1-Ni2 98.20(10), N3-Ni2-Ni1 98.92(10), N2-Ni2-N3 163.73(12).

The EPR spectrum of complex **2** was measured at both room temperature and low temperature. In the room-temperature spectrum in DME (Figure S2a in the Supporting Information), besides the ten hyperfine lines ($g=2.004$) resulting from the ligand-centered radicals, there is one more component at $g=2.184$ due to the $\{Ni_2\}^+$ core, which is similar to those observed for some Ni^{I} complexes.[22] As mentioned above, complex **2** adopts a slightly distorted planar geometry, which may lead to more symmetric environment for the N atoms and methyl groups than that in **1**, resulting in the increased overlap of lines in the EPR spectrum. The frozen-solution (77 K) EPR spectrum of **2** (Figure S2b in the Supporting Information) displays two components, $g_{\parallel}=2.032$ and $g_{\perp}=2.010$, for the ligand radical as in the case of **1**. Unfortunately, the signals of the nickel center are unclear. Moreover, DFT calculations revealed that the optimized structure of the quartet state is energetically most favored, thus proving the existence of the $\{Ni_2\}^+$ units and two ligand radicals (see the Supporting Information for details).

[Na(Et$_2$O)]Na[(L$^{\bullet-}$)Ni–NiL^{2-}] (3): Notably, reduction of **1** by 2.0 equiv of Na resulted in the change of the structure type. In contrast to the perpendicular conformation of **1** and **2**, complex **3** shows a coaxial structure in which the ligands coordinate to Ni atoms in the terminally chelating mode, leading to an unsupported Ni–Ni bond (Figure 3). Each Ni atom is three-coordinate at a trigonal-planar geometry with two N atoms from one α-diimine ligand and the other Ni atom (the sum of the angles around Ni is 359.8 and 359.9°, respectively). The two C_2N_2Ni planes form a dihedral angle of 36.5° rather than the parallel orientation, which was observed in the Zn–Zn, Mg–Mg, and Al–Al-bonded compounds with the doubly reduced ligand L^{2-}.[17] Another interesting structural feature of complex **3** is that the two redox-active α-diimine ligands are in different oxidation

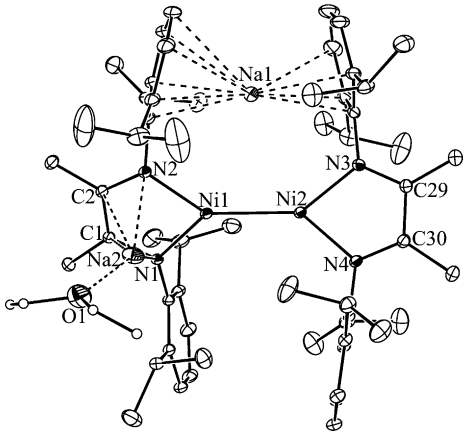

Figure 3. Molecular structure of **3** (thermal ellipsoids are set at the 20% probability level; solvent molecules and hydrogen atoms have been omitted and C atoms on Et_2O drawn as smaller spheres for clarity). Selected bond lengths [Å] and angles [°]: Ni1–Ni2 2.4553(5), Ni1–N1 1.927(2), Ni1–N2 1.954(2), Ni2–N3 1.946(2), Ni3–N4 1.941(2), Ni1···Na1 3.3230(16), Ni2···Na1 3.3071(16), Ni1···Na2 2.7178(17), Na1–O 2.292(4), N1–C1 1.411(4), C1–C2 1.369(4), N2–C2 1.410(4), N3–C29 1.355(4), C29–C30 1.425(4), N4–C30 1.325(4), N1-Ni1-N2 83.07(10), N3-Ni2-N4 80.39(10), Na1-Ni1-Ni2 124.49(4).

states. As judged from the C–N and C–C bond lengths of the NCCCN moiety, one of the ligands retains the monoanionic π radical ($L^{\bullet-}$) form as in **1**, whereas the other one has been reduced to a closed-shell enediamide (L^{2-}; C–N: 1.410(4)/1.411(4) Å and C–C: 1.369(4) Å). Thus, this complex displays a rather asymmetric structure containing not only a mixed-valent [$Ni^{I}Ni^{0}$] core but also mixed oxidation states of the ligands ($L^{\bullet-}/L^{2-}$). The extra negative charges of the ligands are counterbalanced by two Na^{+} cations in different coordination modes. One sodium ion (Na1) interacts with the flanking aryl rings from two ligands in an η^4/η^6 fashion, which is similar to some metal–metal-bonded species.[23] The other sodium ion (Na2) is solvated by a diethyl ether molecule and is η^4-bonded to the enediamido (L^{2-}) ligand, as was observed in many complexes containing dianionic diimine ligands.[11e,17a,b,24] Notably, the monoanionic ligand does not bind a sodium ion. The Ni–Ni bond length in **3** (2.4553(5) Å) is obviously longer than that in **2** (2.3383(14) Å), although both of them own a mixed-valent [$Ni^{I}Ni^{0}$] core. This may be due to the formation of the six-membered ring (NiNCCNNi) in **2** reducing the Ni–Ni interatomic distance.

The EPR spectra of **3** have been measured at both room temperature and low temperature (77 K), which demonstrated the electronic structure of complex **3** to have [$Ni^{I}Ni^{0}$] center and $L^{\bullet-}/L^{2-}$ ligands. The room-temperature spectrum in Et_2O appears as an asymmetric 13-lined signal ($g=2.013$) which is well resolved and can be explained as originating from the sextets (due to two nonequivalent ^{14}N nuclei, $I=1$) and septets (due to six equivalent ^{1}H nuclei of the two methyl groups, $I=1/2$) of the ligand radical $L^{\bullet-}$. This experimental signal matches well the simulated one (Figure 4). Moreover, a broad signal was observed which is attributable to the nickel centers (Figure S3 in the Supporting Information).[11e] The assignment is further proven by its frozen-solution EPR spectrum (Figure 5). In addition to the $g=2.012$ signal resulting from the ligand-centered radical, the g values of 2.270, 2.152 and 2.070 have also been detected, which are typical for Ni^{I} complexes.[25] The small g anisotropy in

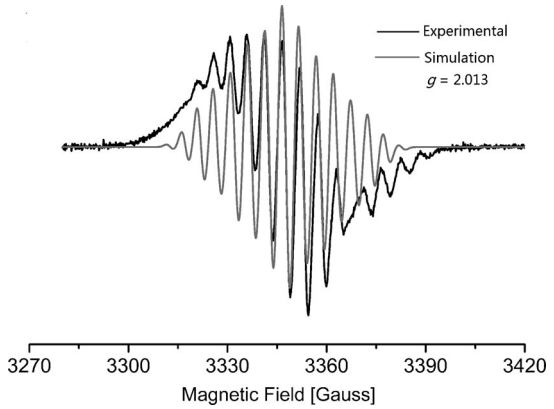

Figure 4. X-band EPR spectrum of [$Na(Et_2O)$]Na[($L^{\bullet-}$)Ni–NiL^{2-}] (**3**) in Et_2O at room temperature. The dark gray line is simulated with the g value as indicated.

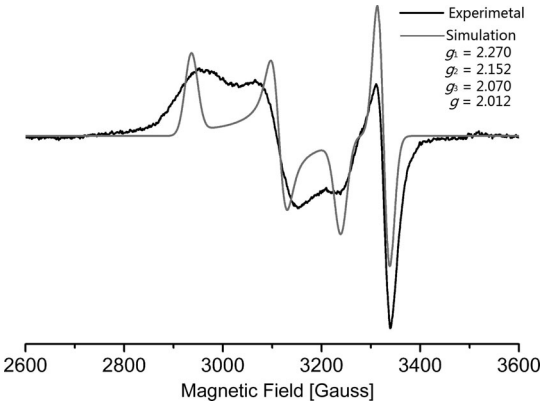

Figure 5. X-band EPR spectrum of [$Na(Et_2O)$]Na[($L^{\bullet-}$)Ni–NiL^{2-}] (**3**) in Et_2O at 77 K. The dark gray line is simulated with g values as indicated.

complex **3** may be due to the exchange interactions of the two Ni centers delocalizing the electron density, which is also supported by DFT calculations (vide infra).

[$Na(Et_2O)]_2Na[L^{2-}$Ni–NiL^{2-}] (4): Reduction of **3** with 1.0 equiv of Na afforded complex **4**, which shows a centrosymmetric dimeric structure (Figure 6). Similar to **3**, the ligands coordinate to Ni atoms in the common terminal-che-

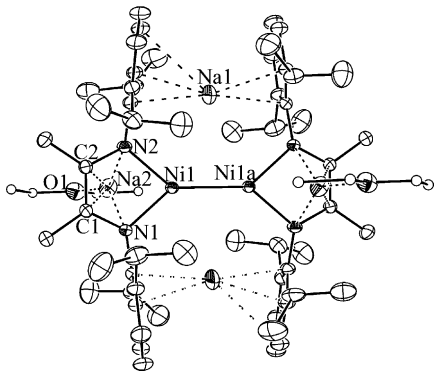

Figure 6. Molecular structure of **4** (thermal ellipsoids are set at the 20% probability level; hydrogen atoms have been omitted and C atoms on Et_2O drawn as smaller spheres for clarity). Selected bond lengths [Å] and angles [°]: Ni1–Ni1a 2.4649(8), Ni1–N1 1.965(2), Ni1–N2 1.962(3), Ni1···Na1 3.150(5), Ni1a···Na1 3.166(5), Ni1···Na2 2.7398(16), Na2–O 2.296(3), N1–C1 1.420(4), C1–C2 1.350(4), N2–C2 1.415(4), N1-Ni1-N2 82.84(10), N1-Ni1-Ni1a 138.47(7), N2-Ni1-Ni1a 138.60(8), Na2-Ni1-Ni1a 128.34(4). Symmetry code a): $1-x,1-y,-z$.

lating fashion (coaxial), and each Ni atom is three-coordinate in a trigonal-planar geometry (the sum of the angles around Ni is 359.9°). The Ni atom deviates slightly (by 0.32 Å) from the C_2N_2 plane, and the two C_2N_2 planes adopt a parallel but not coplanar orientation (the vertical distance is 1.08 Å between the two planes), which is different from the slightly twisted conformation in **3**. To the best of our knowledge, the coaxial complexes **3** and **4** represent the first structurally characterized molecular compounds containing an unsupported Ni–Ni bond with low-valent and low-coordi-

nate Ni centers (the Ni···Na separations between the aryl-sandwiched sodium ion and the nickel atoms are in the range of 3.15–3.30 Å).

Upon acquisition of one electron, the mixed ligands ($L^{\bullet -}$/L^{2-}) in **3** have been reduced to two L^{2-} dianions, whereas the initial monovalent $\{Ni_2\}^+$ core is retained, which is supported by the small *g* anisotropy (2.340, 2.235 and 2.103) of the EPR spectrum (Figure S4 in the Supporting Information) of **4** in solid state at 77 K. In this complex, there is one more Na^+ ion than in **3**, and each ligand binds a solvated $[Na(Et_2O)]^+$ (Na2) locating above and below the enediamide L^{2-} moieties, respectively. The third Na^+ ion (Na1) is also sandwiched by two aryl rings from two ligands as in complex **3**. However, due to the crystal imposed inversion symmetry, this sodium atom is distributed to two positions (on the opposite sides of the Ni–Ni bond) with 50% occupancy each. The Na1···C(aryl) distances range from 2.455(6) to 3.100(6) Å. The Ni–Ni bond length of 2.4649(8) Å in **4** is the longest among these α-diimine Ni–Ni-bonded complexes. Nevertheless, it is shorter than that found at room temperature in nickel metal (2.492 Å). Furthermore, longer Ni–Ni bond lengths in bridged complexes, such as 2.510(2) Å in $Ni_2(CO)_4(\mu\text{-}PPh_2)_2$,[14b] 2.541(2) Å in [($L^H$Ni–Ni$L^H$)(μ-*trans*-diene)],[26] and even 2.596 Å in [Na(tmeda)][{Ni(C_2H_4)$_2$}$_2$(μ-H)][11a] have also been reported.

In complexes **1**–**4**, the Ni–Ni bond length elongates gradually, from 2.2957(6) (**1**) and 2.3383(14) Å (**2**) to 2.4553(5) (**3**) and 2.4649(8) Å (**4**). This can be attributed to the varying coordinate fashion and oxidation state of the nickel metal. As mentioned above, the Ni–Ni distance of the $\{Ni_2\}^+$ core in **2** is slightly longer than that of the higher-oxidation state $\{Ni_2\}^{2+}$ complex **1**, which has the similar perpendicular structure. Meanwhile, bearing the same $\{Ni_2\}^+$ core and similar coaxial coordination geometry, the Ni–Ni bond lengths in **3** and **4** are almost identical. However, the difference between the two types of structure appears to be more distinct, with the coaxial Ni–Ni length being much longer than the perpendicular analogue, as discussed above in the case of complexes **2** and **3**. This is in accord with the literature report of very short metal–metal bonds observed in the perpendicular complexes.[4,7] On the other hand, the effects of these factors are also reflected in the Ni–N bond lengths, which show a similar increase from 1.832 Å in **1** and 1.812 Å in **2** to 1.944 and 1.962 Å in **3** and **4**, respectively. Similar trends have also been reported in the manganese compounds.[6]

DFT studies on the perpendicular and coaxial structures: It is worth noting that in this work the stepwise reduction of a dibromo nickel(II) precursor can be achieved by the amount of Na metal, which was controlled to provide one electron per [$Ni_2(L^{\bullet -})_2$] unit in each step. During the process, both the nickel metal and the ligands were potentially reducible, thus yielding a series of Ni–Ni-bonded compounds with interesting structures and electronic properties. In particular, two different types of structures (perpendicular and coaxial) were formed in the Ni–Ni-bonded compounds.

In order to get deeper insight into the electronic structures and the Ni–Ni bonding nature in the complexes, as well as to better understand the isomerization of the perpendicular and coaxial structures, DFT computations were carried out at the B3LYP/6-31g* level. Complex **1** (perpendicular) and a slightly simplified model of complex **3** (coaxial), [Na(H_2O)]Na[($L^{\bullet -}$)Ni–NiL^{2-}] (**3′**), in which the Et_2O molecule was replaced by H_2O, were chosen as the representatives for the two geometries. Accordingly, the hypothetical models of the contrary structures, **1b** (coaxial, Figure S5 in the Supporting Information) and **3b** (perpendicular, Figure S6 in the Supporting Information) were also optimized for the comparison of the energy differences between the two structural motifs.

DFT geometry optimizations were carried out on complex **1** in the singlet ($S=0$), triplet ($S=1$), and quintet ($S=2$) spin states, and the results indicate that the triplet spin state is energetically most favored, which is consistent with the EPR spectra showing biradical of the two ligands. The optimized triplet-state structure (Table S1 in the Supporting Information) is very close to the experimental data of **1**, except that the Ni–Ni bond length is slightly under-estimated (2.2034 Å) compared with the X-ray diffraction result (2.2957(6) Å). A natural population analysis (NPA) assigned +0.76 natural charges on one nickel center and +0.75 on the other, which is in agreement with the formal oxidation state +1 of the nickel ions. The Wiberg bond index gave a Ni–Ni bond order of 0.54. The Ni–Ni bond is formed mainly by the 4s and 3d orbitals, with 29.7% s, 1.2% p, and 69.1% d characters, as revealed by the natural bond orbital (NBO) analysis. Figure 7 shows the Ni–Ni σ-bond interaction. On the other hand, computations on the hypothetical coaxial model **1b** by the same methods used for **1** were also performed in the triplet ground state. The results indicate that complex **1** is much more stable than **1b** (by about 35 kcal mol^{-1}), which explains the formation of the perpendicular structure **1** rather than the coaxial one in the context of two monoanionic π radical ($L^{\bullet -}$) ligands.

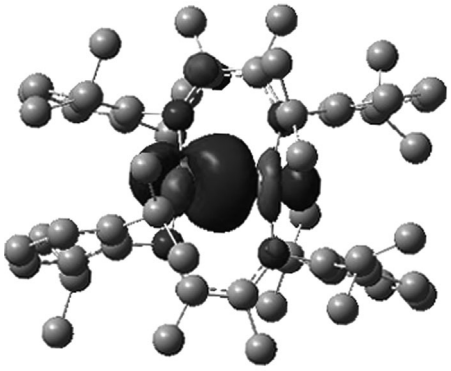

Figure 7. The Ni–Ni σ-bonding orbital (HOMO−18) of complex **1**.

As mentioned above in the crystal structural analysis, complex **3** not only shows a different structure type (co-

axial) from **1** (perpendicular) but also has significantly different oxidation states of the metal centers and ligands. In **3**, one monoanionic π radical ligand and a mixed-valent $[Ni^{I}Ni^{0}]$ core are present, whereas complex **1** contains two monoanionic radical ligands and a diamagnetic $[Ni^{I}Ni^{I}]$ core. Thus, geometry optimizations of **3′** were performed in the triplet ground state (based on its EPR spectra with one ligand radical and one Ni^{I} ion). In the optimized structure of **3′**, the theoretical Ni–Ni bond length (2.4528 Å) is well comparable with the X-ray data for **3** (2.4553(5) Å). The Wiberg bond index gave a Ni–Ni bond order of 0.88. NPA indicated that the natural charges are +0.42 and +0.51 on the two Ni centers, which is in agreement with the mixed-valent $\{Ni_2\}^{+}$ core. The Ni–Ni NBOs were computed for α and β spins with 0.89 occupancies (Table 1), and the Ni–

Table 1. The Ni–Ni natural bond orbitals of compound **3′**.

Spin	Occupancy	%	Ni(1)	%	Ni(2)
α	0.89	46.84	$4s^{0.89}4p^{0.04}3d^{0.06}$	53.16	$4s^{0.91}4p^{0.05}3d^{0.03}$
β	0.89	47.16	$4s^{0.80}4p^{0.06}3d^{0.13}$	52.84	$4s^{0.80}4p^{0.07}3d^{0.12}$

Ni σ bond is formed mainly by the 4s orbitals of the nickel atoms with trace amounts of 4p and 3d characters, as illustrated in HOMO−2 (Figure 8). Furthermore, its hypothetical perpendicular counterpart **3b**, $[Na(Et_2O)]Na[Ni(\mu\text{-}L^{\bullet-})(\mu\text{-}L^{2-})]$, was studied in the triplet ground state. However, the structure **3b** is unstable and cannot be optimized, and many attempts of computation converged to the contrary coaxial analogue **3′**, which further confirms the experimental results of isolation of the coaxial structure when one monoanionic π radical ligand was reduced to the dianion L^{2-}.

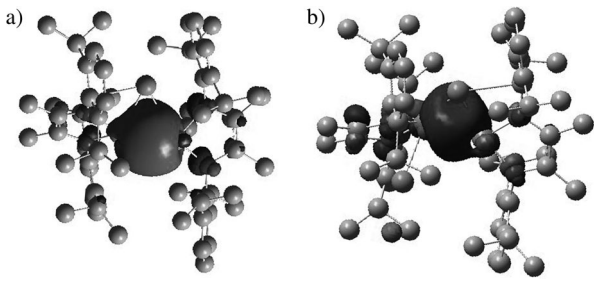

Figure 8. The Ni–Ni σ-bonding orbital of the model compound **3′**. a) The α spin orbital (HOMO−2); b) the β spin orbital (HOMO−2).

The transformation of the perpendicular structure to the coaxial geometry upon reduction has been reported previously for some metal–metal-bonded compounds, such as the Zn–Zn and Mn–Mn bonds. Possible intermediates were suggested by theoretical calculations, and the $[L'MnMnL']^{-}$ species was isolated.[6] In the present dinickel complexes, DFT computations also support the change of the geometry during the course of stepwise reduction of the nickel complex precursor with alkali metal. It is noticeable that the electronic structures and bonding nature of complexes **1** and **3** differ remarkably not only in the bond order but also in the orbital components.

Conclusion

In summary, four Ni–Ni-bonded compounds (**1**–**4**) stabilized by reduced α-diimine ligands have been synthesized by stepwise reduction of the dibromo precursor $LNiBr_2$. The compounds comprise of different oxidation states of both the nickel metal and the redox non-innocent α-diimine ligands, which was characterized by their crystal structures, EPR spectra, and DFT computations. Most interestingly, two distinctly different structure types for the dinickel core are formed: the perpendicular structure (**1** and **2**) and the coaxial structure (**3** and **4**), which have significant effects on the Ni–Ni bond length. DFT calculations were carried out to shed light to the Ni–Ni bonding nature of the compounds, as well as the energy differences of the two structure types.

Experimental Section

General considerations: All manipulations with air- and moisture-sensitive compounds were carried out under argon with standard Schlenk or drybox techniques. The solvents (DME, toluene, Et_2O, and hexane) were dried by using appropriate methods and were distilled under argon prior to use. The EPR spectra of the paramagnetic compounds were recorded on a Bruker EMX-10/12 spectrometer. IR spectra were recorded (thin film on KBr plate) using a Nicolet AVATAR 360 FT-IR spectrometer. Elemental analyses were performed with an Elementar VarioEL III instrument. Compound $LNiBr_2$[18] was prepared according to published procedures.

$[\{Ni(\mu\text{-}L^{\bullet-})\}_2]$ (1): $LNiBr_2$ (0.310 g, 0.50 mmol) and sodium (0.023 g, 1.00 mmol) were combined with Et_2O (30 mL) at room temperature. The mixture was stirred for 2 days with the color change from purple to green. All volatiles were removed in vacuo and the residue was extracted with hexane. The extract was filtered, concentrated to about 8 mL and stored at room temperature. Green crystals (0.104 g, 43%) of $[\{Ni(\mu\text{-}L^{\bullet-})\}_2]\cdot$0.5 hexane were isolated after 2 weeks. EPR (Et_2O, room temperature): $g=2.014$; EPR (solid, 77 K): $g_{\parallel}=2.044$, $g_{\perp}=2.012$; IR (KBr): $\tilde{\nu}=$ 1638, 1576, 1434, 1360, 1323, 1256, 1184, 1114, 932, 752 cm^{-1}; elemental analysis calcd (%) for $C_{59}H_{87}N_4Ni_2$ (969.73): C 73.07, H 9.04, N 5.78; found: C 72.56, H 9.38, N 5.67.

$[Na(DME)_3][\{Ni(\mu\text{-}L^{\bullet-})\}_2]$ (2): $[\{Ni(\mu\text{-}L^{\bullet-})\}_2]\cdot$0.5 hexane (complex **1**, 0.242 g, 0.25 mmol) and Na (0.006 g, 0.25 mmol) were suspended in mixed solvents (20 mL, Et_2O/DME = 3:1), and the mixture was stirred for 1 day at room temperature, resulting in a color change from green to dark-green. After filtration and concentration of the filtrate to approximately 6 mL, the solution was stored at room temperature for several days to yield **2** as dark-green crystals (crystal yield: 0.100 g, 31%). EPR (DME, room temperature): $g=2.184$ and $g=2.004$; EPR (solid, 77 K): $g_{\parallel}=2.032$, $g_{\perp}=2.010$ and broad signals; IR (KBr): $\tilde{\nu}=1640$, 1574, 1436, 1378, 1320, 1250, 1188, 1109, 974, 853, 785, 739, 681 cm^{-1}; elemental analysis calcd (%) $C_{72}H_{120}N_4O_7NaNi_2$ (1294.12): C 66.82, H 9.35, N 4.33; found: C 66.10, H 9.62, N 4.43.

$[Na(Et_2O)]Na[(L^{\bullet-})Ni\text{–}NiL^{2-}]$ (3): Complex **3** was synthesized by the same procedure as reported above for **2** by employing 2.0 equiv of Na (0.012 g, 0.50 mmol) and extraction with toluene. Black-purple crystals of $[Na(Et_2O)]Na[(L^{\bullet-})Ni\text{–}NiL^{2-}]\cdot$toluene (0.104 g, 36%) were isolated after 2 weeks. EPR (Et_2O, room temperature): $g=2.013$, and broad weak signals; EPR (Et_2O, 77 K): $g_1=2.270$, $g_2=2.152$, $g_3=2.070$, and $g=2.012$; IR

(KBr): $\tilde{\nu}$ = 1642, 1568, 1431, 1380, 1323, 1256, 1076, 1022, 933, 853, 792, 731, 677 cm^{-1}; elemental analysis calcd (%) $C_{67}H_{98}N_4ONa_2Ni_2$ (1162.91): C 71.26, H 8.49, N 4.82; found: C 70.43, H 8.54, N 4.43.

$[Na(Et_2O)]_2Na[L^{2-}Ni{-}NiL^{2-}]$ (4): Complex **4** was synthesized by the same procedure as reported for **3** by employing 3.0 equiv of Na (0.018 g, 0.75 mmol). Black-purple crystals of $[Na(Et_2O)]_2Na[L^{2-}Ni{-}NiL^{2-}]$ (0.088 g, 31%) were isolated after 2 weeks. EPR (solid state, 77 K): g_1 = 2.340, g_2 = 2.235, g_3 = 2.103; IR (KBr): $\tilde{\nu}$ = 1584, 1431, 1380, 1323, 1256, 1076, 1022, 933, 853, 792, 731, 677 cm^{-1}; elemental analysis calcd (%) $C_{64}H_{100}N_4O_2Na_3Ni_2$ (1143.86): C 67.20, H 8.81, N 4.89; found: C 66.81, H 8.54, N 4.43. Note: Compound **4** can also be obtained in a 42% isolated yield by treating **3** with 1 equiv of sodium.

X-ray crystallography: Diffraction data for **1**–**4** were collected on a Bruker SMART APEX II diffractometer at 150 K with graphite-monochromated $Mo_{K\alpha}$ radiation (λ = 0.71073 Å). An empirical absorption correction by using SADABS[27] was applied for all data. The structures were solved by direct methods using the SHELXS program.[28] All non-hydrogen atoms were refined anisotropically by full-matrix least squares on F^2 by the use of the SHELXL program. The hydrogen atoms bonded to carbon were included in idealized geometric positions with thermal parameters equivalent to 1.2 times those of the atom to which they were attached. Due to considerable disorder of the solvent in the structure of **3**, the SQUEEZE subroutine of PLATON was employed. CCDC-896901 (**1**), 896902 (**2**), 896903 (**3**) and 896904 (**4**) contain the supplementary crystallographic data for this paper. These data can be obtained free of charge from The Cambridge Crystallographic Data Centre via www.ccdc.cam.ac.uk/data_request/cif.

Acknowledgements

This work was supported by the National Natural Science Foundation of China (Grant No. 20972169 and 21273170).

[1] F. A. Cotton, N. F. Curtis, C. B. Harris, B. F. G. Johnson, S. J. Lippard, J. T. Mague, W. R. Robinson, J. S. Wood, *Science* **1964**, *145*, 1305–1307.

[2] a) S. P. Green, C. Jones, A. Stasch, *Science* **2007**, *318*, 1754–1757; b) R. West, M. J. Fink, J. Michl, *Science* **1981**, *214*, 1343–1344; c) A. Sekiguchi, R. Kinjo, M. Ichinohe, *Science* **2004**, *305*, 1755–1757; d) I. Resa, E. Carmona, E. Gutierrea-Puebla, A. Monge, *Science* **2004**, *305*, 1136–1138.

[3] a) Y. C. Tsai, D. Y. Lu, Y. M. Lin, J. K. Hwang, J. S. K. Yu, *Chem. Commun.* **2007**, 4125–4127; b) Y. Wang, B. Quillian, P. Wei, H. Wang, X.-J. Yang, Y. Xie, R. B. King, P. v. R. Schleyer, H. F. Schaefer III, G. H. Robinson, *J. Am. Chem. Soc.* **2005**, *127*, 11944–11945; c) Z. Zhu, M. Brynda, R. J. Wright, R. C. Fischer, W. A. Merrill, E. Rivard, R. Wolf, J. C. Fettinger, M. M. Olmstead, P. P. Power, *J. Am. Chem. Soc.* **2007**, *129*, 10847–10857; d) J. Chai, H. Zhu, A. C. Stückl, H. W. Roesky, J. Magull, A. Bencini, A. Caneschi, D. Gatteschi, *J. Am. Chem. Soc.* **2005**, *127*, 9201–9206.

[4] a) K. A. Kreisel, G. P. A. Yap, O. Dmitrenko, C. R. Landis, K. H. Theopold, *J. Am. Chem. Soc.* **2007**, *129*, 14162–14163; b) A. Noor, F. R. Wagner, R. Kempe, *Angew. Chem.* **2008**, *120*, 7356–7359; *Angew. Chem. Int. Ed.* **2008**, *47*, 7246–7249; c) C. W. Hsu, J. S. K. Yu, C. H. Yen, G. H. Lee, Y. Wang, Y. C. Tsai, *Angew. Chem.* **2008**, *120*, 10081–10084; *Angew. Chem. Int. Ed.* **2008**, *47*, 9933–9936; d) A. Noor, G. Glatz, R. Müller, M. Kaupp, S. Demeshko, R. Kempe, *Z. Anorg. Allg. Chem.* **2009**, *635*, 1149–1152; e) Y. C. Tsai, Y. M. Lin, J. S. K. Yu, J. K. Hwang, *J. Am. Chem. Soc.* **2006**, *128*, 13980–13981; f) L. Fohlmeister, S. Liu, C. Schulten, B. Moubaraki, A. Stasch, J. D. Cashion, K. S. Murray, L. Gagliardi, C. Jones, *Angew. Chem.* **2012**, *124*, 8419–8423; *Angew. Chem. Int. Ed.* **2012**, *51*, 8294–8298.

[5] T. Nguyen, A. D. Sutton, M. Brynda, J. C. Fettinger, G. J. Long, P. P. Power, *Science* **2005**, *310*, 844–847.

[6] D. Y. Lu, J. S. K. Yu, T. S. Kuo, G. H. Lee, Y. Wang, Y. C. Tsai, *Angew. Chem.* **2011**, *123*, 7753–7757; *Angew. Chem. Int. Ed.* **2011**, *50*, 7611–7615.

[7] a) C. Jones, C. Schulten, L. Fohlmeister, A. Stasch, K. S. Murray, B. Moubaraki, S. Kohl, M. Z. Ertem, L. Gagliardi, C. J. Cramer, *Chem. Eur. J.* **2011**, *17*, 1294–1303; b) E. Nelkenbaum, M. Kapon, M. S. Eisen, *Organometallics* **2005**, *24*, 2645–2659.

[8] Y. Xie, H. F. Schaefer III, R. B. King, *J. Am. Chem. Soc.* **2005**, *127*, 2818–2819.

[9] K. Fischer, K. Jonas, P. Misbach, R. Stabba, G. Wilke, *Angew. Chem.* **1973**, *85*, 1001–1012; *Angew. Chem. Int. Ed. Engl.* **1973**, *12*, 943–1026.

[10] *Nickel and Its Surprising Impact in Nature, in Metal Ions in Life Science Vol. 2* (Eds.: A. Sigel, H. Sigel, R. K. O. Sigel), Wiley, Chichester, **2007**.

[11] a) K. R. Pörschke, W. Kleimann, G. Wilke, K. H. Claus, C. Krüger, *Angew. Chem.* **1983**, *95*, 1032–1033; *Angew. Chem. Int. Ed. Engl.* **1983**, *22*, 991–992; b) M. J. Tenorio, M. C. Puerta, P. Valerga, *J. Chem. Soc. Dalton Trans.* **1996**, 1305–1308; c) S. Pfirrmann, C. Limberg, C. Herwig, C. Knispel, B. Braun, E. Bill, R. Stösser, *J. Am. Chem. Soc.* **2010**, *132*, 13684–13691; d) T. Matsumoto, T. Nagahama, J. Cho, T. Hizume, M. Suzuki, S. Ogo, *Angew. Chem.* **2011**, *123*, 10766–10768; *Angew. Chem. Int. Ed.* **2011**, *50*, 10578–10580; e) Q. Dong, Y. Zhao, Y. Su, J. H. Su, B. Wu, X. J. Yang, *Inorg. Chem.* **2012**, *51*, 13162–13170.

[12] a) L. R. Byers, L. F. Dahl, *Inorg. Chem.* **1980**, *19*, 680–692; b) J. J. Maj, A. D. Rae, L. F. Dahl, *J. Am. Chem. Soc.* **1982**, *104*, 3054–3063; c) C. H. Lee, D. S. Laitar, P. Mueller, J. P. Sadighi, *J. Am. Chem. Soc.* **2007**, *129*, 13802–13803; d) H. Einspahr, J. Donohue, *Inorg. Chem.* **1974**, *13*, 1839–1843.

[13] a) M. Ito, T. Matsumoto, K. Tatsumi, *Inorg. Chem.* **2009**, *48*, 2215–2223; b) D. A. Vicic, W. D. Jones, *J. Am. Chem. Soc.* **1999**, *121*, 7606–7617; c) C. H. Wei, L. F. Dahl, *Inorg. Chem.* **1970**, *9*, 1878–1887.

[14] a) R. A. Jones, A. L. Stuart, J. L. Atwood, W. E. Hunter, R. D. Rogers, *Organometallics* **1982**, *1*, 1721–1723; b) J. A. J. Jarvis, R. H. B. Mais, P. G. Owston, D. T. Thompson, *J. Chem. Soc. A* **1970**, 1867; c) R. A. Jones, N. C. Norman, M. H. Seeberger, J. L. Atwood, W. E. Hunter, *Organometallics* **1983**, *2*, 1629–1634; d) B. Kesanh, D. R. Gardner, B. Scott, B. W. Eichhorn, *J. Chem. Soc. Dalton Trans.* **2000**, 1291–1296.

[15] a) Y. Chen, C. Sui-Seng, D. Zargarian, *Angew. Chem.* **2005**, *117*, 7899–7903; *Angew. Chem. Int. Ed.* **2005**, *44*, 7721–7725; b) A. Velian, S. Lin, A. J. M. Miller, M. W. Day, T. Agapie, *J. Am. Chem. Soc.* **2010**, *132*, 6296–6297.

[16] As determined from a survey of the Cambridge Crystallographic Database in August, **2012**.

[17] a) X.-J. Yang, J. Yu, Y. Liu, Y. Xie, H. F. Schaefer, Y. Liang, B. Wu, *Chem. Commun.* **2007**, 2363–2365; b) Y. Liu, S. Li, X.-J. Yang, P. Yang, B. Wu, *J. Am. Chem. Soc.* **2009**, *131*, 4210–4211; c) Y. Liu, S. Li, X.-J. Yang, P. Yang, J. Gao, Y. Xia, B. Wu, *Organometallics* **2009**, *28*, 5270–5272; d) P. Yang, X.-J. Yang, J. Yu, Y. Liu, C. Zhang, Y. H. Deng, B. Wu, *Dalton Trans.* **2009**, 5773–5779; e) Y. Zhao, Y. Liu, L. Yang, J. G. Yu, S. Li, B. Wu, X.-J. Yang, *Chem. Eur. J.* **2012**, *18*, 6022–6030; f) J. Gao, S. Li, Y. Zhao, B. Wu, X.-J. Yang, *Organometallics* **2012**, *31*, 2978–2985.

[18] L. K. Johnson, C. M. Killian, M. Brookhart, *J. Am. Chem. Soc.* **1995**, *117*, 6414–6415.

[19] M. M. Khusniyarov, K. Harms, O. Burghaus, J. Sundermeyer, *Eur. J. Inorg. Chem.* **2006**, 2985–2996.

[20] a) M. G. Gardiner, G. R. Hanson, M. J. Henderson, F. C. Lee, C. L. Raston, *Inorg. Chem.* **1994**, *33*, 2456–2461; b) P. J. Bailey, R. A. Coxall, C. M. Dick, S. Fabre, S. Parsons, L. J. Yellowlees, *Chem. Commun.* **2005**, 4563–4565; c) P. J. Bailey, C. M. Dick, S. Fabre, S. Parsons, L. J. Yellowlees, *Dalton Trans.* **2006**, 1602–1610; d) J. Gao, Y. Liu, Y. Zhao, X.-J. Yang, Y. Sui, *Organometallics* **2011**, *30*, 6071–6077.

[21] K. Chłopek, E. Bothe, F. Neese, T. Weyhermüller, K. Wieghardt, *Inorg. Chem.* **2006**, *45*, 6298–6307.

[22] a) J. F. Berry, E. Bothe, F. A. Cotton, S. A. Ibragimov, C. A. Murillo, D. Villagrán, X. Wang, *Inorg. Chem.* **2006**, *45*, 4396–4406; b) F. A. Cotton, M. Matusz, R. Poli, X. Feng, *J. Am. Chem. Soc.* **1988**, *110*, 1144–1154.

[23] a) Z. Zhu, R. J. Wright, M. M. Olmstead, E. Rivard, M. Brynda, P. P. Power, *Angew. Chem.* **2006**, *118*, 5939–5942; *Angew. Chem. Int. Ed.* **2006**, *45*, 5807–5810; b) L. Pu, A. D. Phillips, A. F. Richards, M. Stender, R. S. Simons, M. M. Olmstead, P. P. Power, *J. Am. Chem. Soc.* **2003**, *125*, 11626–11636.

[24] a) Y. Liu, Y. Zhao, X.-J. Yang, S. Li, J. Gao, P. Yang, Y. Xia, B. Wu, *Organometallics* **2011**, *30*, 1599–1606; b) Y. Liu, P. Yang, J. Yu, X.-J. Yang, J. D. Zhang, Z. Chen, H. F. Schaefer, B. Wu, *Organometallics* **2008**, *27*, 5830–5835.

[25] M.-E. Pandelia, H. Ogata, L. J. Currell, M. Flores, W. Lubitz, *Biochim. Biophys. Acta* **2010**, *1797*, 304–313.

[26] R. Diercks, L. Stamp, J. Kopf, H. tom Dieck, *Angew. Chem.* **1984**, *96*, 891–895; *Angew. Chem. Int. Ed. Engl.* **1984**, *23*, 893–894.

[27] G. M. Sheldrick, SADABS: Area-Detector Absorption Correction; University of Göttingen, **1996**.

[28] G. M. Sheldrick, SHELXL-97: Programs for Crystal Structure Analysis; University of Göttingen, **1997**.

Received: June 26, 2013
Published online: October 2, 2013

